Available online at www.sciencedirect.com
ScienceDirect
Journal of the European Ceramic Society 29 (2009) 2411–2417
www.elsevier.com/locate/jeurceramsoc

Sintering, high temperature strength and oxidation resistance of liquid-phase-pressureless-sintered SiC–AlN ceramics with addition of rare-earth oxides

Giuseppe Magnani [a,*], Francesco Antolini [b], Leandro Beaulardi [b], Emiliano Burresi [c], Antonino Coglitore [b], Claudio Mingazzini [b]

[a] *ENEA, Department of Physics Technologies and New Materials, Bologna Research Center, Via dei Colli 16-40136 Bologna, Italy*
[b] *ENEA, Department of Physics Technologies and New Materials, Faenza Research Center, Via Ravegnana 186-48018 Faenza, Italy*
[c] *ENEA, Department of Physics Technologies and New Materials, Bologna Research Center, Via Martiri di Monte Sole 2-40100 Bologna, Italy*

Received 9 November 2008; received in revised form 15 December 2008; accepted 24 December 2008
Available online 8 February 2009

Abstract

SiC–AlN composites can be pressureless sintered with the addition of rare-earth oxides (RE = Y, Yb, Er, Lu, Ho, Sm, Ce) and without protective powder bed. Sintered bodies showed high density (≥97% T.D.) and were mainly composed by 2H SiC–AlN solid solution with additive containing grain boundary phases. The high temperature strength and oxidation resistance of the composites were also investigated and correlated with the cationic radii of the oxide additives. The flexural strength at 1500 °C increased from 269 MPa to 587 MPa as direct consequence of the rare-earth cationic radius decrease. The specific weight gain during oxidation at 1500 °C for 200 h showed the same behaviour, decreasing from 12.60 mg/cm^2 to 3.13 mg/cm^2.

Keywords: Sintering; Composites; Mechanical Properties; SiC; Rare-earth oxides

1. Introduction

Liquid-phase sintered (LPS) silicon carbide is a candidate material for high temperature structural components. Sintering additives such as Al_2O_3–Y_2O_3 and AlN–Y_2O_3 were extensively used to obtain fracture resistant LPS–SiC ceramics.[1–4] In the case of SiC–AlN–Y_2O_3 composites, previous studies reported that 2H SiC–AlN solid solution with improved high temperature properties could be achieved with SiC/AlN weight ratio greater than 80/20 and above 1850 °C.[1,2] With SiC/AlN weight ratio of 50/50, densification is achieved by liquid-phase sintering using metal oxides such as yttria (Y_2O_3) as the sintering additives.[3] This oxide reacts with SiO_2 and Al_2O_3 which are always present at the surface, respectively, of SiC and AlN particles, to form an oxynitride melt, $Y_{10}Al_2Si_3O_{18}N_4$.[4]

A problem associated with the use of additives is the resultant degradation of high temperature properties due to residual grain boundary glassy phase.[5] Several attempts to prevent the observed degradation in the high temperature properties have been reported.[6–10] These include the use of different types of sintering additives in order to change the crystalline nature of the grain boundary phases in which these additives reside. For example silicon carbide ceramics containing AlN and Er_2O_3,[7,9] Lu_2O_3,[7,8,10] Sc_2O_3,[7,10,11] Sm_2O_3,[6] Yb_2O_3[6,12] as sintering-aids were reported to show favourable high temperature properties and oxidization resistance, with SiC–AlN–Er_2O_3, SiC–AlN–Lu_2O_3 and SiC–AlN–Sc_2O_3 systems resulting in the best performance at high temperature due to the higher eutectic temperature of the grain boundary phases, $RE_2Si_2O_7$ (RE = Er, Lu, Sc) compared to oxynitride phases. All these studies are focused on SiC–AlN–RE_2O_3 ceramics with high SiC content (79–99 wt%) and sintered by hot-pressing or gas-pressure sintering, while studies on the effects of the nature of the grain boundary phases on the high temperature behaviour of pressureless-sintered 2H SiC–AlN composites have not been published yet. Our purpose was to examine the effectiveness of seven rare-earth oxides (Y_2O_3, Er_2O_3, Ho_2O_3, Lu_2O_3, Sm_2O_3, Yb_2O_3, CeO_2) as densification aids for SiC (50 wt%)–AlN

* Corresponding author.
E-mail address: giuseppe.magnani@bologna.enea.it (G. Magnani).

0955-2219/$ – see front matter © 2009 Elsevier Ltd. All rights reserved.
doi:10.1016/j.jeurceramsoc.2008.12.020

Table 1
Characteristics of the starting powders.

Powder	Purity (wt%)	Specific surface area (m^2/g)	Particle size (μm)
α-SiC	>97.0	15.6	0.48
AlN	>98.0	3.3	0.1–0.5
Y_2O_3	99.9		<5
Lu_2O_3	99.9		<5
Er_2O_3	99.9		<5
Yb_2O_3	99.9		<5
CeO_2	99.0		<5
Ho_2O_3	99.9		<5
Sm_2O_3	99.9		<5

(50 wt%) ceramics sintered by an innovative pressureless process without protective powder bed. Another important purpose was to investigate how the sintering additives and, hence, the intergranular phase chemistry influence the mechanical properties and oxidation resistance of the SiC–AlN composites.

2. Experimental procedure

Commercially available α-SiC (UF10, H.C. Starck, Germany), AlN (Grade F, Tokuyama Soda, Japan), Y_2O_3 (H.C. Starck, Germany), Er_2O_3, Ho_2O_3, Lu_2O_3, Sm_2O_3, Yb_2O_3 (Cerac Inc., USA) and CeO_2 (Sigma–Aldrich, Switzerland) were used as starting powders. Characteristics of these powders are reported in Table 1.

A batch of each powder composed by 48 wt% SiC–48 wt% AlN–4 wt% RE_2O_3 was wet-mixed in ethanol for 12 h using SiC grinding balls. After drying and sieving, the powder was compacted by die pressing at 67 MPa and subsequently was pressed at 150 MPa by CIP.

Sintering was always performed in a graphite element furnace in flowing nitrogen at 1 atm with green bodies put inside a graphite crucible without protective powder bed. Sintering was performed at 1950 °C, while an annealing step of 4–6 h was conducted at 2050 °C. Thermal cycle was characterised by heating and cooling rate of 20–30 °C/min and by dwell time of 0.5 h at the sintering temperature.

The bulk densities of the sintered samples were determined using the Archimede method. The microstructures were characterized using scanning electron microscopy (SEM), while X-ray patterns (XRD), were collected with a Philips powder diffractometer, with a Bragg–Brentano geometry, equipped with a Copper anode operated at 40 kV and 30 mA, step 0.02°, time 6 s. The phase analysis was carried out with the PC X'pertHigh Score software Version 2.2a (PANalyical B.V., Almelo, The Netherlands).

Oxidation experiments were carried out at 1500 °C over a period of 200 h in air. Rectangular pellets (18 mm × 3 mm × 3 mm) were prepared from the bulk specimens with a diamond saw. After grinding to reduce superficial roughness, the specimens were cleaned in an ultrasonic bath and degreased with acetone and ethanol. Dried samples were then weighed and the exact dimensions were measured in order to calculate the surface area. The experiments were conducted in a furnace having molybdenum disilicide heating elements.

Finally, flexural strength was determined by four-point bend tests at 1500 °C (ten samples for each composition). Samples as bars of 2 mm × 2.5 mm × 25 mm were prepared and tested in accordance with the standard ENV 843-1 (crosshead speed 0.5 mm/min).

3. Results and discussion

3.1. Sintering mechanism and microstructure

Bulk density and crystalline phases of the sintered samples are reported in Table 2. The sintered densities of SiC–AlN ceramics were found to be ≥97% of the theoretical density as calculated by the rule of mixtures. Hence, the proposed oxide sintering-aids are suitable for the densification of SiC–AlN composites. In fact, thermodynamic calculations confirmed the stability of SiC in the presence of the studied RE_2O_3 during thermal treatment.[13] At the same time decomposition of AlN at the sintering temperature was efficiently suppressed by a N_2 atmosphere.[14]

Rare-earth oxides participate to the formation of the liquid phase that assists densification during pressureless sintering[3] and precipitates at the grain boundary during cooling. A core-rim microstructure was put in evidence by plasma-etching as a consequence of a solution and reprecipitation mechanism with larger grains of free-SiC growing at the expense of smaller ones (Fig. 1).

Grain boundary phases such as $Y_{10}Al_2Si_3O_{18}N_4$ with Y_2O_3 addition[4] and $RE_4Si_2N_7O_2$/$RE_2Si_3N_4O_3$ with RE = Er, Lu, Ho, Sm, Yb[9,12,15,16] as sintering-aids were formed after sintering. Cerium oxide (CeO_2) promotes densification following a more complex mechanism. On the basis of previous study based on the hot-pressing of Si_3N_4–CeO_2 system,[17] it can be hypothesised that during the pressureless sintering pro-

Table 2
Density (%T.D.) and crystalline phases of the SiC–AlN–RE_2O_3 composites (mp = main phase, sp = secondary phase, gbp = grain boundary phase, tr = trace).

Material	Bulk density (%T.D.)	Crystalline phases
SiC–AlN–Y_2O_3	97	2H SiC–AlN (mp), α-SiC (sp), $Y_{10}Al_2Si_3O_{18}N_4$ (gbp), α-Cristobalite (tr)
SiC–AlN–Lu_2O_3	98	2H SiC–AlN (mp), α-SiC (sp), Lu_2O_3 (gbp), $Lu_2Si_2O_7$ (gbp), α-Cristobalite (tr)
SiC–AlN–Er_2O_3	99	2H SiC–AlN (mp), α-SiC (sp) Er_2O_3 (gbp), $Er_2Si_2O_7$ (gbp)
SiC–AlN–Ho_2O_3	99	2H SiC–AlN (mp), α-SiC (sp), Ho_2O_3 (gbp), $Ho_2Si_2O_7$ (gbp), $Ho_4Si_2N_7O_2$ (tr)
SiC–AlN–Yb_2O_3	98	2H SiC–AlN (mp), α-SiC (sp), Yb_2O_3 (gbp), $Yb_2Si_2O_7$ (gbp), α-Cristobalite (tr)
SiC–AlN–Sm_2O_3	98	2H SiC–AlN (mp), α-SiC (sp), Sm_2O_3 (gbp), $Sm_2Si_2O_7$ (gbp)
SiC–AlN–CeO_2	97	2H SiC–AlN (mp), α-SiC (sp), Ce_2SiO_5 (gbp), $Ce_2Si_2O_7$ (gbp), α-Cristobalite (tr), $Ce_{4.67}(SiO_4)_3O$(tr)

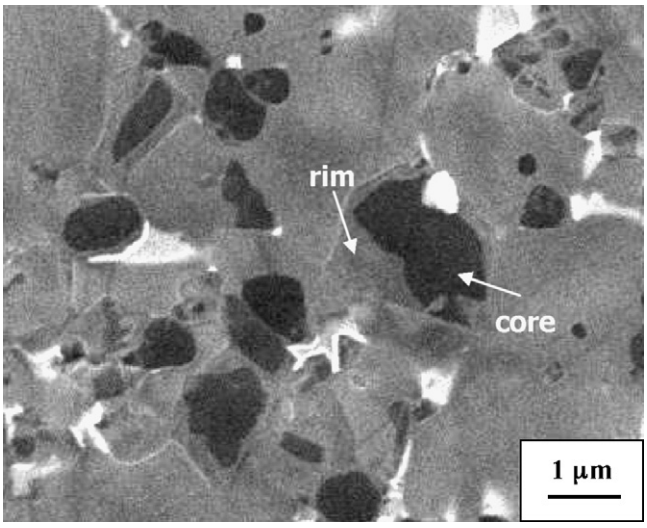

Fig. 1. Microstructure of SiC–AlN–Y_2O_3 showing core-rim structure of the SiC grains.

cess, CeO_2 is mostly reduced to Ce_2O_3 by reaction with SiO_2 located on the surface of SiC particles.[18] XRD analysis of pressureless-sintered SiC–AlN–CeO_2 confirmed that Ce(III)-crystalline phases ($Ce_{4.67}(SiO_4)_3O$ and $Ce_2Si_6N_8O_3$) were formed as grain boundary phases (Fig. 2). In addition, residual $Ce_{4.67}(SiO_4)_3O$ was found in the annealed SiC–AlN–CeO_2 ceramics where Ce_2SiO_5 and $Ce_2Si_2O_7$ were also detected as consequence of the decomposition of $Ce_{4.67}(SiO_4)_3O$ and $Ce_2Si_6N_8O_3$ (Fig. 2 and Table 2). According to the XRD pattern reported in Fig. 2, the majority of intergranular phases were

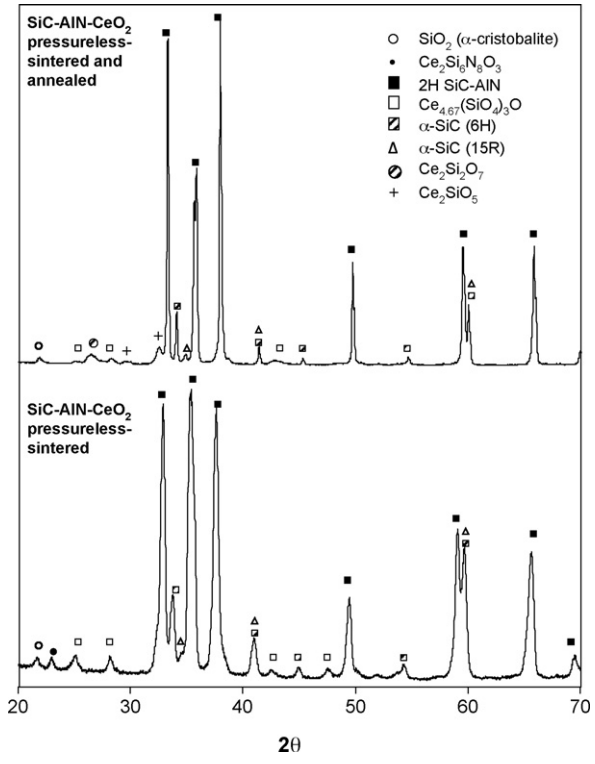

Fig. 2. XRD pattern of SiC–AlN–CeO_2 composites before and after annealing (2050 °C × 4 h).

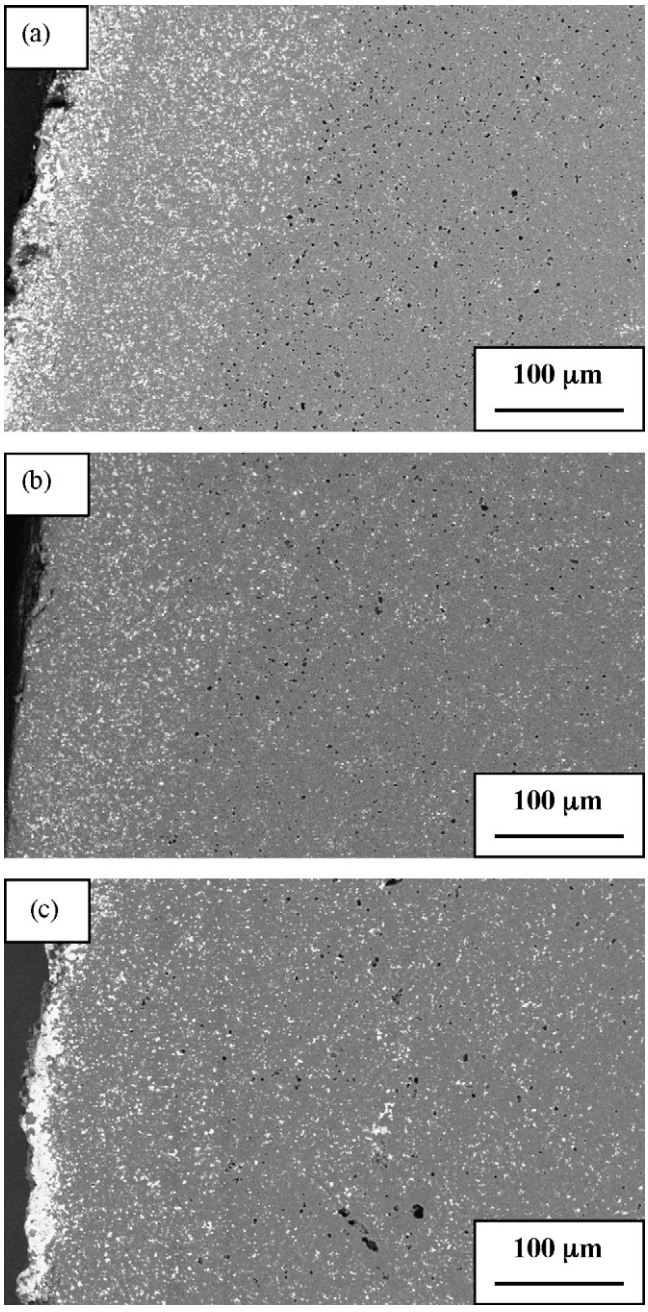

Fig. 3. SEM images of SiC–AlN–Y_2O_3 after an annealing time of (a) 1 h, (b) 2 h and (c) 4 h.

Table 3
Flexural strength at 1500 °C and RE^{3+} radius values of the SiC–AlN–RE_2O_3 composites.

Material	Flexural strength at 1500 °C (MPa)	Cationic radius of RE^{n+} (10^{-1} nm)
SiC–AlN–Y_2O_3	479	1.019
SiC–AlN–Lu_2O_3	521	0.977
SiC–AlN–Er_2O_3	587	1.004
SiC–AlN–Yb_2O_3	430	0.985
SiC–AlN–CeO_2	286	1.140
SiC–AlN–Ho_2O_3	400	1.015
SiC–AlN–Sm_2O_3	423	1.079

crystalline in as-sintered and annealed materials showing sharp reflections in the XRD pattern, clear indication of the low amount of residual amorphous phases. In any case, additional work will be needed in order to evaluate the amount of amorphous phases as a function of the cationic radius of the oxide additives.

Upon annealing, the oxynitride phases ($RE_4Si_2N_7O_2$/$RE_2Si_3N_4O_3$) slowly decompose to oxide/silicate (RE_2O_3/$RE_2Si_2O_7$) phases[15] (Table 2). Furthermore, secondary phases are expelled from the grain boundary region upon annealing, and very small amounts of residual secondary phases remain at the grain boundary. The reduction of residual secondary phases occurs due to the volatilisation of these phases via carbothermal reductions (graphite-heated furnace).[19] Movement of liquid phase from the grain boundary to the surface has been already shown by Lee et al. in SiC–YAG composites[20] which presented a porous reaction-layer of 90 μm on the outside region

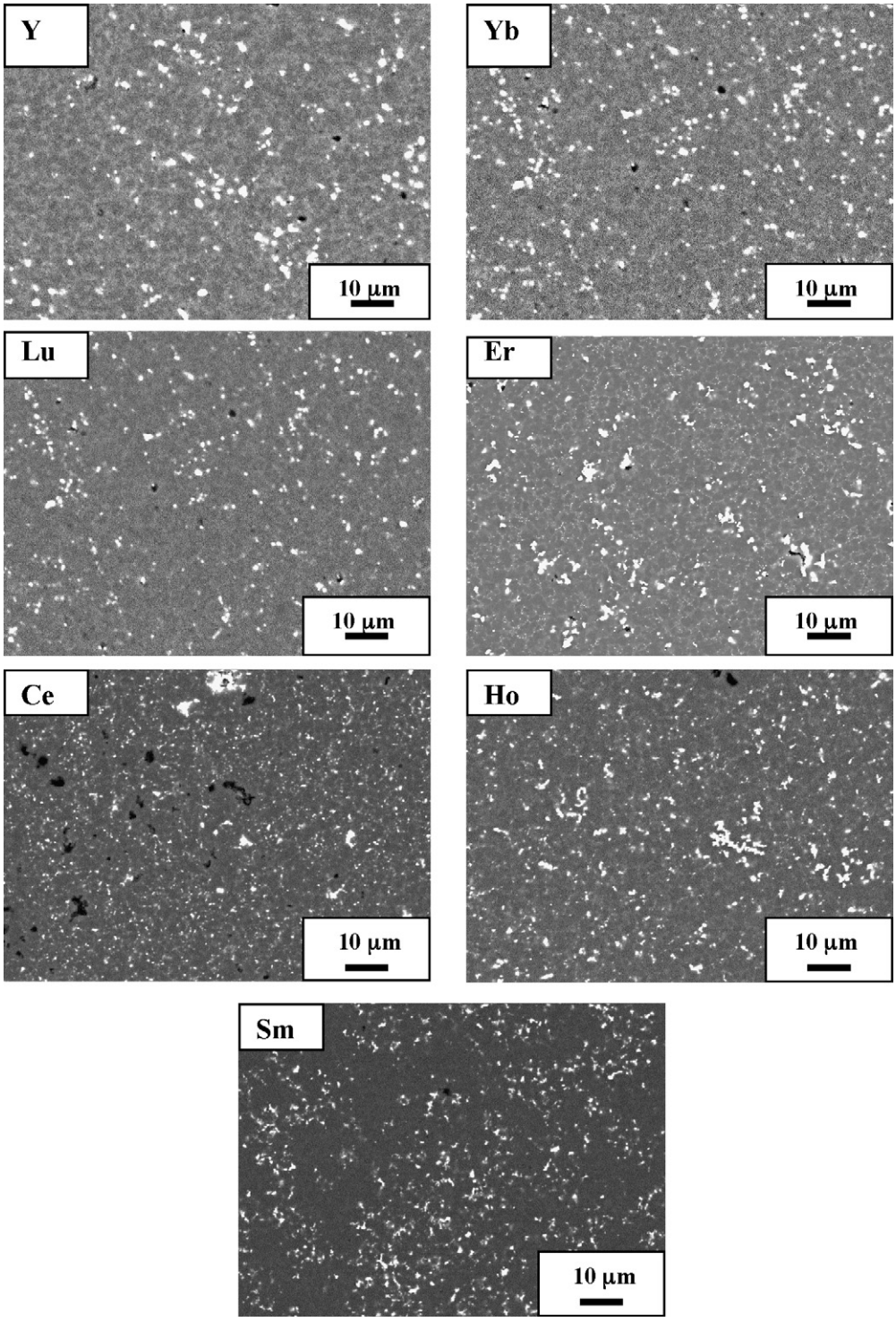

Fig. 4. SEM images of the microstructure of the SiC–AlN–RE_2O_3 (RE = Y, Yb, Er, Lu, Ho, Sm, Ce) ceramics after pressureless sintering and annealing.

of the specimens. Fig. 3 shows typical behaviour of the grain boundary phases during thermal annealing of sintered SiC–AlN ceramics. SEM micrographs reported here are relative to the SiC–AlN–Y_2O_3 system and clearly demonstrate that the grain boundary phase ($Y_{10}Al_2Si_3O_{18}N_4$) melts during annealing and moves in the direction of low Gibbs free energy, i.e. the surface, where it volatilises as SiO or Al_2O.[21]

After annealing, residual grain boundary phase is homogenously distributed in the samples. Images reported in Fig. 4 and obtained with back-scattered electrons put in evidence the bright spots of the liquid phase in the SiC–AlN–RE_2O_3 composites.

3.2. Mechanical properties

The flexural strength values measured at 1500 °C on sintered specimens are presented in Table 3. The highest strength of 587 MPa was obtained with the SiC–AlN–Er_2O_3 ceramics, while SiC–AlN–Ho_2O_3 ceramics showed lower strength values as compared to the others. The variation of the high temperature strength with the radius of the cation in the oxide additive is shown in Fig. 5. The cationic radii used in this study are listed in Table 3.[22] As shown, the high temperature strength of SiC–AlN–RE_2O_3 ceramics is strongly dependent on the cationic radius of the oxide additive. A similar correlation between the ionic radius of rare-earth oxides additives and mechanical properties was also observed in the case of liquid-phase sintered SiC–Al_2O_3–RE_2O_3,[23] hot pressed SiC–AlN–RE_2O_3[6] and hot pressed Si_3N_4–$RE_2Si_2O_7$[24] ceramics. In these studies the difference in the mechanical properties was attributed to the chemistry of the intergranular phases. Shelby et al.[25] firstly reported that the physical properties of rare-earth aluminosilicate glasses, such as glass transformation temperature and thermal expansion coefficient, varied linearly with the ionic radius of the rare-earth ions. Similarly, the rare-earth ions might play a major structural role in intergranular phases found in the SiC–AlN ceramics. Since the RE^{3+} ions are all trivalent, their field strength (the effective force to attract neighbouring anions) varies with the reciprocal of the ionic radius. So, the smaller RE^{3+} ions made the network more compact and tight and, consequently, produced stronger intergranular phases. Under such conditions, the stronger grain boundary would result in higher flexural strength of ceramics.

3.3. Oxidation behaviour

Fig. 6 is a plot of weight gain per unit surface area as a function of time at 1500 °C. All materials had specific weight gains on the order of 2–7 mg/cm^2 after 200 h with the exception of SiC–AlN–CeO_2 which presented a weight gains of 12 mg/cm^2 after the same time at temperature. The oxidation of pressureless-sintered SiC–AlN–RE_2O_3 has been shown to obey a parabolic rate law of the type:

$$\Delta W^2 = kt \quad (1)$$

where ΔW is the specific weight gain, k is the kinetic constant of parabolic oxidation and t is the oxidation time.

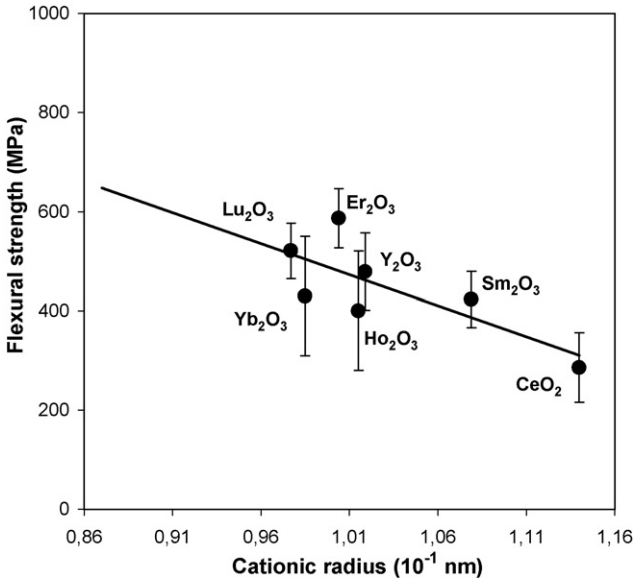

Fig. 5. High temperature strength as function of RE^{3+} radius.

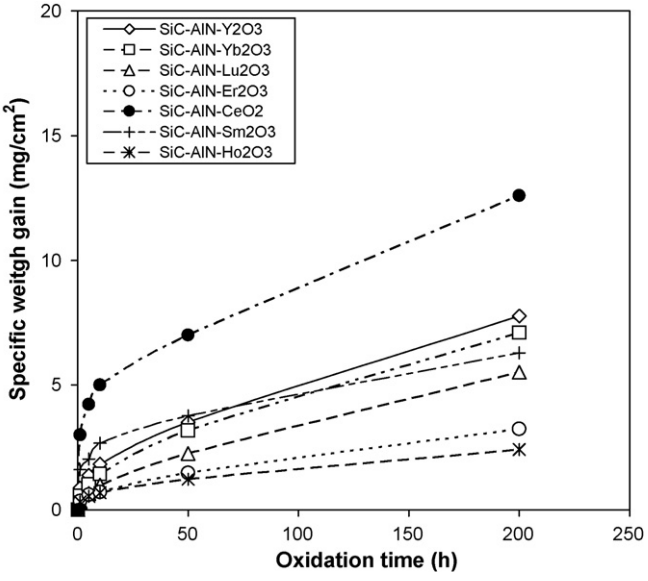

Fig. 6. Specific weight gain as function of the oxidation time (T = 1500 °C).

Table 4
Specific weight gains and constants rate of the different SiC–AlN–RE_2O_3 ceramics after oxidation at 1500 °C for 200 h.

Material	Specific mass gain (mg/cm^2)	Rate constant (mg^2/(cm^4 h))
SiC–AlN–Y_2O_3	7.77	2.99×10^{-1}
SiC–AlN–Lu_2O_3	5.52	1.49×10^{-1}
SiC–AlN–Er_2O_3	3.25	5.22×10^{-2}
SiC–AlN–Yb_2O_3	7.09	2.49×10^{-1}
SiC–AlN–CeO_2	12.6	7.47×10^{-1}
SiC–AlN–Ho_2O_3	3.13	4.92×10^{-2}
SiC–AlN–Sm_2O_3	6.29	1.86×10^{-1}

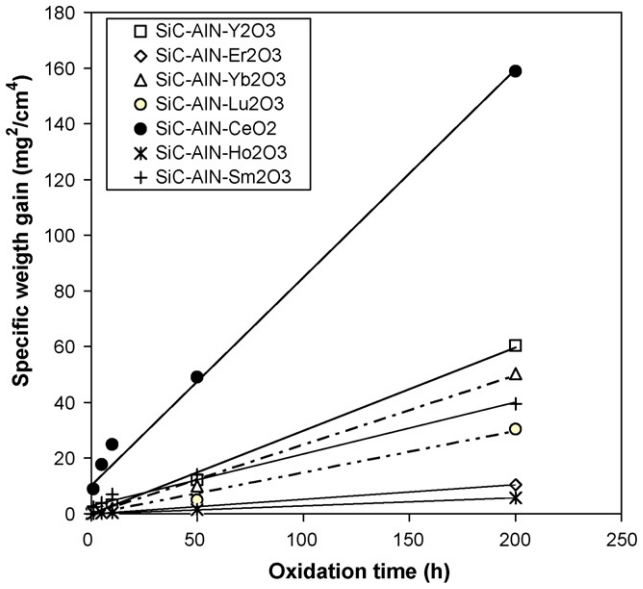

Fig. 7. Square of the specific weight gain as function of the oxidation time ($T = 1500\,^{\circ}C$).

Plotting these data, results in straight lines for all curves are shown in Fig. 7. Table 4 contains the parabolic oxidation rate constants (slope of the straight lines) for the seven compositions investigated, as well as the total specific weight gains after 200 h. The parabolic oxidation behaviour of these ceramics indicates a diffusive process as the rate-limiting step associated with the migration of additive cations (RE^{3+}) towards the interface between ceramic and the surface oxide.[26]

The high oxidation resistance of these materials, demonstrated by the values of specific weight gains of Table 4, can be attributed both to a minimal amount of amorphous grain boundary phases, with high viscosity due to the presence of refractory RE^{3+}, and to thermodynamically stable crystalline secondary phases, such that the driving force for additive cation diffusion to the surface is minimized.

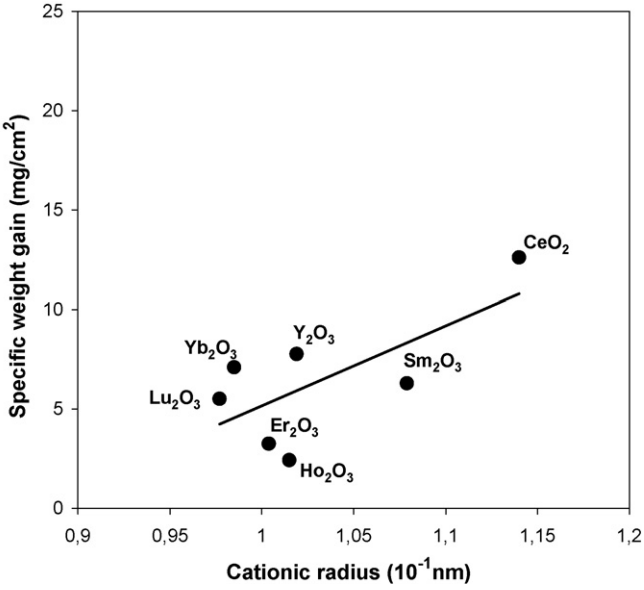

Fig. 8. Specific weight gain as function of RE^{3+} radius.

In addition, a greater refractory nature of the amorphous grain boundary phase is expected for those materials sintered with the oxide additives having a smaller cationic radius.[24] As a consequence it was observed that the specific weight gains of the specimens during oxidation were dependent on the cationic radius of the oxide additives (Fig. 8).

4. Conclusion

SiC–AlN composites can be obtained by pressureless-sintering process with different RE_2O_3 (RE = Y, Yb, Er, Lu, Ho, Sm, Ce) as densification-aids and without protective powder bed. The main characteristics of the sintered samples are:

1. The microstructure presents SiC grains, showing a core-rim structure, dispersed into a matrix composed by solid solution 2H SiC–AlN. Rare-earth oxides form oxynitride species, which precipitate at the grain boundary and decompose during annealing at high temperature to produce silicate phases ($RE_2Si_2O_7$).
2. High temperature strength reaches the highest value (587 MPa) with SiC–AlN–Er_2O_3 composites. A strong dependence between flexural strength and cation radius of the rare-earth oxides has been also showed. Smaller RE^{3+} ions produce stronger intergranular phases, which leads to a higher flexural strength of SiC–AlN ceramics.
3. Pressureless-sintered SiC–AlN–RE_2O_3 composites show a high oxidation resistance at 1500 °C. In particular, SiC–AlN–Ho_2O_3 and SiC–AlN–Er_2O_3 exhibit the lowest values of specific weight gain after oxidation at 1500 °C for 200 h. Oxidation always follows a parabolic rate law with migration of RE^{3+} ions as rate-limiting step. In addition, cationic radius of the oxide additives greatly influence the oxidation resistance of the different SiC–AlN–RE_2O_3 ceramics due to the different level of refractoriness of the residual amorphous grain boundary phase.

References

1. Zangvil, A. and Ruh, R., Phase relationship in the silicon carbide–aluminum nitride system. *J. Am. Ceram. Soc.*, 1988, **71**(10), 884–890.
2. Lim, C. S., Effect of a-SiC on the microstructure and toughening of hot-pressed SiC–AlN solid solution. *J. Mater. Sci.*, 2000, **35**, 3029–3035.
3. Magnani, G. and Beaulardi, L., Properties of liquid phase pressureless sintered SiC–based materials obtained without powder bed. *J. Aust. Ceram. Soc.*, 2005, **41**(1), 31–36.
4. Magnani, G. and Beaulardi, L., Mechanical properties of pressureless sintered SiC–AlN composites obtained without sintering bed. *Ceram. Eng. Sci. Proc.*, 2004, **25**(4), 31–36.
5. Magnani, G., Minoccari, G. L. and Pilotti, L., Flexural strength and toughness of liquid phase sintered silicon carbide. *Ceram. Int.*, 2000, **26**(5), 495–500.
6. Balog, M., Sedlackova, K., Zifcak, P. and Janega, J., Liquid phase sintering of SiC with rare-earth oxides. *Silikaty*, 2005, **49**(4), 259–262.
7. Kim, Y. W., Chun, Y. S., Lee, S. H., Park, J. Y., Nishimura, T., Mitomo, M. and Ryu, W. S., Microstructure and mechanical properties of heat-resistant silicon carbide ceramics. *Key Eng. Mater.*, 2007, **336–338**, 1409–1413.

8. Biswas, K., Rixecker, G. and Aldinger, F., Effect of rare-earth cation additions on the high temperature oxidation behaviour of LPS–SiC. *Mater. Sci. Eng. A*, 2004, **374**(1–2), 56–63.
9. Guo, S., Hirosaki, N., Tanaka, H., Yamamoto, Y. and Nishimura, T., Oxidation behaviour of liquid-phase sintered SiC with AlN and Er_2O_3 additives between 1200 °C and 1400 °C. *J. Eur. Ceram. Soc.*, 2003, **23**, 2023–2029.
10. Choi, H. J., Kim, Y. W., Mitomo, M., Nishimura, T., Lee, J. H. and Kim, D. Y., Intergranular glassy phase free SiC ceramics retains strength at 1500 °C. *Scr. Mater.*, 2004, **50**, 1203–1207.
11. Kim, Y. W., Lee, S. H., Nishimura, T. and Mitomo, M., Heat resistant silicon carbide with aluminium nitride and scandium oxide. *Acta Mater.*, 2005, **53**, 4701–4708.
12. Izhevskyi, V. A., Bressiani, A. H. A. and Bressiani, J. C., Effect of liquid phase sintering on microstructure and mechanical properties of Yb_2O_3–AlN containing SiC-based ceramics. *J. Am. Ceram. Soc.*, 2005, **88**(5), 1115–1121.
13. Rafaniello, W., Cho, K. and Virkar, A., Fabrication and characteristics of SiC–AlN alloys. *J. Mater. Sci.*, 1981, **16**, 3479–3488.
14. Biswas, K., Rixecker, G., Wiedmann, I., Schweizer, M., Upadhyaia, G. S. and Aldinger, F., Liquid phase sintering and microstructure-property relationships of silicon carbide ceramics with oxynitride additives. *Mater. Chem. Phys.*, 2001, **67**, 180–191.
15. Biswas, K., Schneider, J., Rixecker, G. and Aldinger, F., Comparative bending creep behaviour of silicon carbide sintered with oxynitride additives. *Scr. Mater.*, 2005, **53**, 591–596.
16. Biswas, K., Liquid phase sintering of SiC ceramics with rare earth sesquioxides, Doctoral thesis, University of Stuttgart, 2002.
17. Guha, J. P., Goursat, P. and Billy, M., Hot-pressing and oxidation behaviour of silicon nitride with ceria additive. *J. Am. Ceram. Soc.*, 1980, **63**(1–2), 119–120.
18. Guo, G. F., Li, J., Kong, X. Y., Lin, H., Liang, L., He, M., Yang, L., Wu, J. and Cui, B., Direct measurement of residual stresses and their effects on the microstructure and mechanical properties of heat-treated Si_3N_4 ceramics II: with CeO_2 as a single additive. *Acta Mater.*, 2007, **55**, 3245–3251.
19. Sciti, D., Guicciardi, S. and Bellosi, A., Effect of annealing treatments on microstructure and mechanical properties of liquid-phase-sintered silicon carbide. *J. Eur. Ceram. Soc.*, 2001, **21**(5), 621–632.
20. Lee, J. K., Tanaka, H. and Kim, H., Microstructural changes in liquid-phase sintered α-silicon carbide. *Mater. Lett.*, 1996, **29**, 135–142.
21. Lee, J. K., Tanaka, H. and Kim, H., Movement of liquid phase and the formation of surface reaction layer on the sintering of β-SiC with an additive of yttrium aluminium garnet. *J. Mater. Sci. Lett.*, 1996, **15**, 409–411.
22. Shannon, R. D., Revised effective ionic radii and systematic studies of interatomic distances in halides and chalcogenides. *Acta Cryst.*, 1976, **A32**, 751–767.
23. Zhou, Y., Hirao, K., Toriyama, M., Yamauchi, Y. and Kanzaki, S., Effects of intergranular phase chemistry on the microstructure and mechanical properties of silicon carbide ceramics densified with rare-earth oxide and alumina additions. *J. Am. Ceram. Soc.*, 2001, **84**(7), 1642–1644.
24. Choi, H. J., Lee, J. G. and Kim, Y. W., High temperature strength and oxidation behaviour of hot-pressed silicon nitride-disilicate ceramics. *J. Mater. Sci.*, 1997, **32**, 1937–1942.
25. Shelby, J. E. and Kohli, J. T., Rare-earth aluminosilicate glasses. *J. Am. Ceram. Soc.*, 1990, **73**(1), 39–42.
26. Magnani, G. and Beaulardi, L., Long term oxidation behaviour of liquid phase pressureless sintered SiC–AlN ceramics obtained without powder bed. *J. Eur. Ceram. Soc.*, 2006, **26**, 3407–3413.